Nanoscale

ROYAL SOCIETY OF CHEMISTRY

PAPER

View Article Online
View Journal | View Issue

Cite this: *Nanoscale*, 2020, **12**, 14504

Impact of water on the lubricating properties of hexadecane at the nanoscale†

Clodomiro Cafolla and Kislon Voïtchovsky *

Fluid lubricants are routinely used to reduce friction in a wide range of applications, from car engines to machinery and hard-disk drives. However, their efficiency can be significantly influenced by the ambient conditions they are exposed to, in particular humidity. Our understanding of the molecular mechanisms responsible for the well-documented impact of water on lubrication remains limited, hindering the improvement of tribological formulations. Here, we use Atomic Force Microscopy (AFM) and shear force spectroscopy to investigate the structural and dynamical behaviour of a model lubricant, hexadecane, confined between an AFM probe and a hydrophilic mica surface at different temperatures and humidities. We show that both the nanoscale structure and the tribological behaviour of the system are dominated by the nucleation of water nanodroplets at the interface. The process is favoured at higher temperature and can be explained with classical nucleation theory whereby the droplets become stable when larger than 20 nm to 50 nm size, depending on the ambient conditions. Below this threshold, a molecularly thin film of water molecules coats the surface uniformly. Highly localised shear measurements demonstrate a detrimental impact of the nanodroplets on shear with a twofold increase in the lubricated friction force. However, this can be mitigated by the adjunction of an amphiphilic additive, here oleic acid.

Received 10th May 2020,
Accepted 23rd June 2020

DOI: 10.1039/d0nr03642k

rsc.li/nanoscale

Introduction

Friction and wear are ubiquitous in nature.[1] Tribological contacts have a fundamental role in a wide range of phenomena, from the flow of red blood cells in vessels and capilaries[2] and the motion of joints,[3] to the function of car brakes[4] and wind turbines.[5] Irrespective of length scales considered, the impact of friction on sustainability and our quality of life is profound.[6] It is estimated that about a quarter of all energy consumed worldwide is related to friction[7]. One of the most common and effective approaches to reducing friction and wear is the use of lubricants.[8] Lubricants typically create thin mobile films, often in fluid form, adsorbed at the interface between moving parts. They allow the parts to slide easily and smoothly past each other by confining the shearing-induced molecular rearrangements to the lubricant layer.[7,8] The efficiency of a lubricant depends on many different parameters such as the lubricant's molecular structure and intrinsic properties, the local topography and chemical characteristics of the sliding surfaces,[9] and the operating parameters such as sliding speed,[10,11] contact pressure,[12] and environmental factors such as temperature[10] and humidity.[9] While many of these parameters can be kept to a particular operating regime, certain environmental parameters are significantly harder to control in real-life applications. The ambient humidity, for example, has a marked impact on lubricated friction.[13,14] Atmospheric humidity can vary considerably and uncontrollably over short periods of time but its effects are not easily mitigated due to the fact that the moving parts in most devices do not operate in a controlled atmosphere.[15,16] Water molecules can usually enter the lubricant through several sources including condensation and adsorption from a humid environment, leakage from heat exchangers or as a by-product of chemical reactions.[17,18] The effect of water on the properties of lubricants are often detrimental,[17,18] especially when preventing the adsorption of organic lubricant molecules at the relevant interfaces. The ability of water to displace organic lubricants is particularly pronounced for interfaces involving a hydrophilic solid such as the metal oxide surfaces of most industrial machinery and engines.[14,19] Water can impede the formation of an effective lubricating and protective layer between the sliding surfaces.[17,20–22] Since the thickness of the lubrication film can be as thin as a few nanometers,[23] even trace quantities of water may be detrimental, resulting in increased friction and damage to the moving parts.

Water can bind to the oxygen groups of both the main lubricant molecules and additives.[17,20–22] Aside from displacing organic compounds,[24] water adsorption can lead to the formation of free-radicals which affect the tribochemistry of

Physics Department, Durham University, Durham DH1 3LE, UK.
E-mail: kislon.voitchovsky@durham.ac.uk

† Electronic supplementary information (ESI) available: Supplementary methods and Fig. S1–S7. See DOI: 10.1039/d0nr03642k

the interface, in particular for systems involving metal oxides[20] lubricated by alkane-based products.[14] A broad spectrum of fluid lubricant formulations are currently based on alkanes,[14,25–29] but a full understanding of the impact of humidity on lubricated friction is still elusive due to nanoscale nature of the problem: the adsorption of water molecules and the subsequent impact on lubrication are processes difficult to observe *in situ*, at the molecular level, in a controlled environment (humidity, temperature), all while tracking the system's evolution over relevant periods of time.[9,21,30]

This is precisely the goal of the present study that combines nanoscale atomic force microscopy (AFM) experiments with macroscopic contact angle (CA) measurements all conducted in controlled atmosphere. To make our results as relevant as possible while ensuring a clear interpretation, we investigated the hexadecane-mica model system. Hexadecane is a model mineral base oil and one of the basic components of most commercial organic lubricants.[14,25–27] Mica is a hydrophilic aluminosilicate that acts here as a model metal oxide surface.[12] Mica has been extensively used as a model substrate to study the fundamental aspects of lubricated friction, including real-life applications. Studies have explored lubricants as diverse as commercial additives,[31] hydrated metal ions,[12] ionic liquids[32] and liquid crystals intended as the new generation of lubricants.[33] Here, using mica has three main advantages. First, its layered structure makes it easy to obtain clean, atomically flat surfaces. This makes mica ideal to study the molecular-level details of lubrication because chemical variations across the interface can be clearly differentiated from topographical or roughness effects such as tribological contacts between asperities.[12,24,30,34] Second, mica being an aluminosilicate, it is hydrophilic and contains many of the atoms often present in typical machinery and engines (Al, Si, O).[12] This allows us to conduct experiments that partly replicate the hydrophilic surface chemistry of 'real' systems while discriminating between lubricant and topographical effects. Finally, the fact that mica is a well-established model system for lubrication ensures a more robust interpretation of the experimental results in light of existing literature. Previous experimental studies on mica suggest an orientation of the interfacial hexadecane molecules parallel to the substrate.[35] This is also supported by molecular dynamics and Monte Carlo simulations that reveal well-ordered hexadecane structures when nanoconfined between two mica surfaces.[36,37] The existence of in-plane order and interlayer correlation may result in long-range correlations in the confined film[34] with humidity adversely affecting the hydrocarbon adsoprtion.[38] However, no study to date has been able to clearly visualise water adsorption/desorption due to the high mobility of the water molecules.[38,39] Furthermore, it is still unclear how physically adsorbed water molecules and their distribution on the sliding surfaces may affect the shear response of the lubricant.[30] Most current experimental techniques average over large regions of the interface.[9,30]

Here, we combine *in situ* high-resolution AFM imaging of the interfaces as it evolves with nano-rheological shear measurements at multiple temperature and humidities. This enables us to quantitatively link the nanoscale organisation of water and the lubricant at the interface with the resulting changes in lubricating friction in response to variations of the environment.

Experimental

Sample preparation

The experiments were conducted on high-quality V1 muscovite mica discs (SPI supplies, West Chester, PA, USA) with controls on highly orientated pyrolytic graphite (HOPG) substrates. The mica and HOPG substrates were glued to steel plates using silver paint (Ted Pella Inc, Redding, CA) and cured at 75 °C overnight to ensure optimal thermal conductivity.[12,40] The substrates were freshly cleaved before any experiment. High-performance liquid chromatography-grade hexadecane and oleic acid both with a purity ≥99% were purchased from Sigma-Aldrich (St. Louis, MO, USA) and used without any further purification.

AFM measurements

The measurements were performed on a Cypher ES AFM system (Oxford Instruments, Santa Barbara, CA, USA), equipped with temperature control. The AFM probes used were Arrow UHF silicon nitride cantilevers (Nanoworld, Switzerland) and AD-2.8AS diamond coated silicon cantilevers (Adama Innovations LTD, Dublin, Ireland). The flexural calibration of each cantilever was performed using its thermal spectrum.[41] Arrow cantilevers were found to have a stiffness k_f in the range 1.6–5.0 N m^{-1}, a Q-factor of 3.1 ± 0.3 and a flexural resonance frequency of 1900 ± 1 kHz in hexadecane.[42] The diamond-coated cantilevers had a typical stiffness of k_f = 2.2 ± 0.5 N m^{-1} (in agreement with the nominal value of 2.8 N m^{-1}), a Q-factor of 3.3 ± 0.5 and a resonance frequency of 255 ± 1 kHz both in hexadecane.[42] The torsional resonance frequencies are higher than the flexural resonances, and are hence not relevant for the shear measurements which are conducted at 1.1 kHz. Calibration of the cantilevers' inverse optical lever sensitivity (InvOLS) and torsional spring constant k_t was achieved using the method described elsewhere.[42] We found k_t = 230 ± 30 N m^{-1} for the AD-2.8AS, consistent with the literature.[42]

All experiments were conducted at thermal equilibrium. This was achieved ensuring that the cooling/heating rate of the temperature control system within the AFM was constant for at least 15 minutes. Relative humidity was controlled with nitrogen flux and monitored with a commercial Fluke 971 Thermohygrometer (Fluka Corporation, Washington, USA) placed inside the AFM chamber. Within each set of experiments, we ensured that variations in relative humidty RH < 2%. Each set of experiments (including imaging and spectroscopy) was repeated at least three times in order to confirm data reproducibility. Accurate cleaning procedures were implemented to avoid any source of contamination (see also ESI section S1†).[12]

High-resolution imaging was conducted in amplitude-modulation with the AFM probe completely immersed in hexadecane. The cantilever was acoustically driven at a frequency close to its resonance due to the limitations of photothermal excitation in viscous organic solvents. Away from the substrate, the tip oscillates with a constant amplitude A_0. At the interface the amplitude is reduced due to tip-interface interactions. The sample is raster-scanned keeping a set point amplitude $A_s < A_0$ constant using a feedback loop which constantly readjusts the tip–substrate distance. The topographic image of the interface is obtained from the feedback corrections. The ratio A_s/A_0 was set as high as possible for gentle imaging, with A in the range 0.5–2 nm. The phase lag between the driving oscillation and the tip oscillation varies freely giving information on the probe-sample interactions. This approach allows for probing primarily the interfacial liquid with little direct contact between the tip and the surface of the solid.[12,28,40,43]

Shear-force spectroscopy was used to gain quantitative dynamical insights into the behaviour of the lubricant. Thus, we probed the lubricated friction using an average shearing velocity of 0.5 μm s^{-1}. The AFM is effectively used as a highly localised nanoscopic linear shear rheometer with an amplitude of 0.5 nm, and a frequency of 1.1 kHz, below the natural resonance of the scanner (2 kHz) and of the cantilevers.[28] The method allows probing determined locations of the interface with nanometer lateral precision and a shear force resolution in the pN range.[12] The cantilever vertical deflection, lateral torsional (or shear) amplitude A_t and phase lag with the driving shear are recorded simultaneously from the tip's motion.[12,28] The vertical deflection is used to calculate the confining force and pressure applied by the tip, here ~10 MPa for every nN applied. Given the small torsional amplitudes applied here, we can quantify the magnitude of the shear force F_s as

$$F_S = A_t k_t, \quad (1)$$

The shear phase provides information on the nature of the tip–sample coupling, with $\varphi_S = 0°$ and $\varphi_S = 90°$ corresponding to a perfectly elastic and perfectly viscous behaviour, respectively.[12]

For each set of experiments, shear-force measurements were acquired over at least 5 locations, with at least 20 force curves per location. The results were then averaged. Data analysis was conducted using homemade routines developed in Igor Pro (Wavemetrics, Lake Oswego, OR, USA) and Python. Representative results of the raw output signals are presented in ESI section 1 (Fig. S2†). ESI section 2 (Fig. S3†) shows control experiments to confirm the reliability of the shear phase to study the viscoelasticity of the confined fluid under shear.

Contact angle measurements were conducted in a homemade polycarbonate glove box. The relativity humidity was controlled with a nitrogen flux and monitored with a thermo-hygrometer (Fluka Corporation, Washington, USA) placed within the glove box. The temperature was kept constant using a hot plate (Thermo Fisher Scientific, Waltham, Massachusetts, USA) and monitored with the thermo-hygrometer. Experiments were performed once thermal stability was achieved (temperature and RH variations smaller than 0.1 °C and 2% over at least 30 minutes, respectively). The mica was first cleaved and preconditioned to the desired temperature and RH. Wettability measurements were then carried out by placing a drop (5 μl) of hexadecane on the preconditioned mica while recording its evolution over time in a movie captured with a portable digital microscope Dino-Lite Edge camera (AnMo Electronics Corporation, Taiwan). Simultaneous side-view images of the drop allowed for contact angle quantification. The experiments were repeated two times. Data analysis was conducted using the ImageJ/Fiji free software[44] with the Contact Angle plugin.[45] Further analysis was performed with homemade routines developed in Igor Pro (Wavemetrics, Lake Oswego, OR, USA) and Python.

Results and discussion

Evolution of the mica-hexadecane interface at the nanoscale

We start by exploring the impact of ambient humidity on the nanoscale evolution of the mica-hexadecane interface using high-resolution AFM imaging. A cyclic change in temperature between 25 °C and 95 °C is imposed to the system so as to mimic the typical working conditions of lubricated mechanical system. A representative set of AFM images taken at different temperatures in presented in Fig. 1. As the temperature increases, small round protrusions begin to appear at the interface past 35 °C (arrows in Fig. 1) and increase in number, eventually spreading homogenously across the surface of mica at 95 °C. Interestingly, a hysteresis behaviour can be observed when cooling the system back down to temperatures below 35 °C with the different protrusions not disappearing, but merging instead into larger protrusions tens of nanometres across (Fig. 1). The mobile nature of the protrusions and their ability to coalesce suggest liquid nano-droplets nucleating at the interface. Given the fact that the only two liquids present are hexadecane and traces of water from the ambient humidity, we interpret the protrusions as interfacial water nanodroplets. This interpretation is also consistent with the fact that the surface of mica initially carries a uniform nanoscopic layer of water when first immersed into the hexadecane. This is due to the strong hydrophilicity of the mica surface where a water layer between 0.4–2 nm thick builds up spontaneously and almost instantaneously when mica is cleaved in ambient conditions.[38,39,46] To further support this interpretation, the experiments were repeated at higher (RH > 75%) and lower (RH < 10%) humidity. The results (ESI Fig. S3†) consistently demonstrate a significant increase or reduction of the droplets' size and density. Thorough control experiments and rigorous cleaning procedure rule out the possibility that the protrusions originate from other contaminants and emphasise the need of a hydrophilic surface such as mica for the nanodroplets to form (ESI Figs S3–6†). In contrast, the chemical characteristics of the AFM probe do not seem to play a major role with the

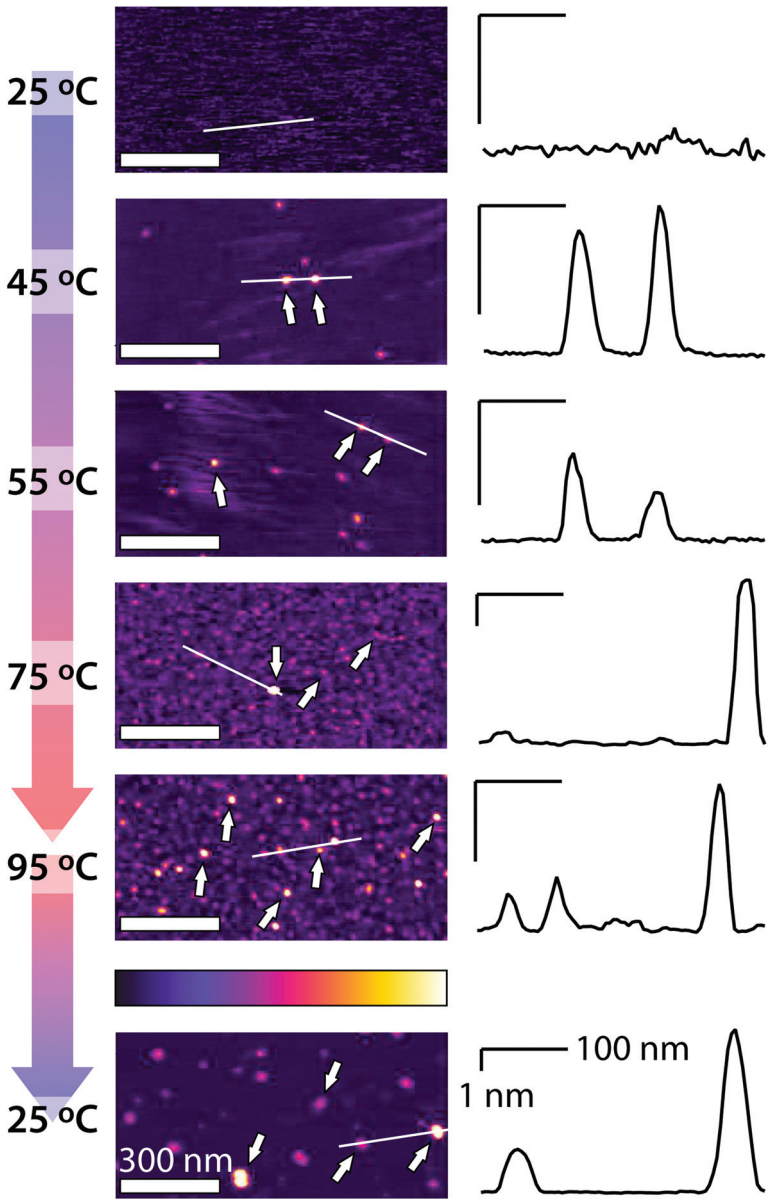

Fig. 1 Impact of temperature on the hexadecane-mica interface at ambient humidty. High-resolution amplitude-modulation AFM images of the hexadecane-mica interface exposed to the ambient atmosphere reveals a smooth and regular interface at 25 °C. As the temperature increases, hemi-spherical protrusions interpreted as water nanodroplets progressively populate the interface (arrows). These nanodroplets are typically 20–50 nm wide and 1–5 nm tall (profiles) with the highest coverage at 95 °C. Upon subsequently lowering the temperature back down to 25 °C, the nano-droplets coalesce into fewer, larger droplets. The experiments were performed at RH = 40 ± 2%.

droplets being present on mica regardless of whether a hydrophilic (Fig. 1) or hydrophobic (Fig. S5†) AFM tip is used. The fact that the flat interface dominates the observation instead of the cantilever-liquid interface is also consistent with previous AFM studies.[47–49]

Rationalising the effect of temperature

In the proposed interpretation of the AFM observations, increasing the temperature stimulates the condensation into nano-droplets of the nanoscopic water film[38,39] that initially covers the mica surface uniformly (Fig. 2a and b). The underlying mechanism can be described in terms of a competition between hexadecane and water molecules for the mica's surface. The affinity between both liquids and the mica surface is best quantified by their respective work of adhesion W. The water-mica and hexadecane-mica works of adhesion in ambient conditions and at 25 °C are given by $W_{w,m} \sim 146$ mN m^{-1} and $W_{h,m} \sim 162$ mN m^{-1}, respectively (ESI section 7 for details†). The difference is relatively small, in the order of 10%. Hexadecane furthermore exhibits a spreading coefficient S almost 5 times larger than water on mica, with $S_{h,m} \sim 100$ mN m^{-1} and $S_{w,m} \sim 20$ mN m^{-1}, respectively (see ESI

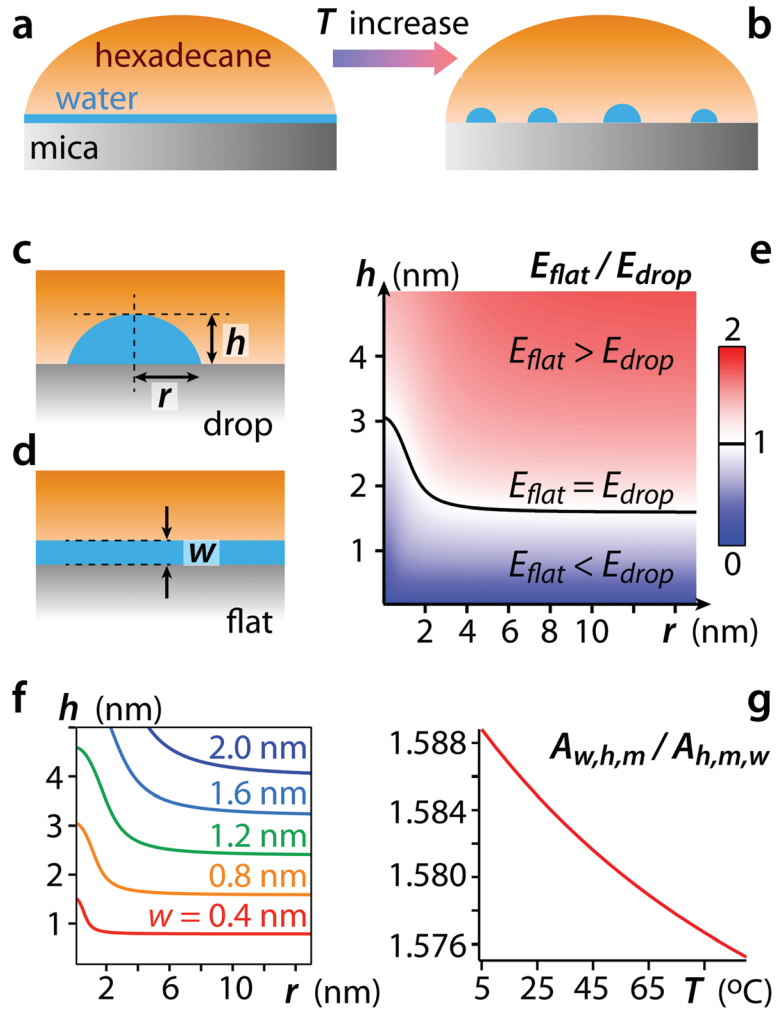

Fig. 2 Thermodynamics of hexadecane and water at the mica interface. A cartoon representation of the interface shows the temperature-stimulated transition from a nanoscopic water film covering the mica surface uniformly inside the hexadecane (a) to nanodroplets of water with hexadecane partially reaching the mica surface (b). It is possible to compare the total interfacial energy associated with a set area of the interface containing either a water nanodroplet (c, energy E_{drop}) or a uniform water film of same volume (d, energy E_{flat}) (see ESI section 7 for details†). The results (e) confirm that droplets become the most stable configuration ($E_{drop} < E_{flat}$) in the size-range observed experimentally. The nucleation threshold ($E_{drop} = E_{flat}$) is shown as a black line. Smaller droplets are unstable, consistent with classical nucleation theory. The ambient humidity affects the thickness w of the initial water film and hence the nucleation threshold (f). The temperature dependence of the ratio between the Hamaker constants describing water-mica interactions in hexadecane H_{whm} and hexadecane-mica interactions in water H_{hwm} (g) supports the idea that a temperature increase comparatively reinforces the van der Waals interactions between the hexadecane and the mica through the interfacial water.[53–59]

section 7 for details†). These values indicate that hexadecane and water are in close competition for the mica surface in ambient conditions, despite the mica being strongly hydrophilic. We also note that freshly cleaved mica can react with atmospheric CO_2 and other carbon contaminants,[38,50,51] enhancing the affinity of hexadecane.

Under these circumstance, simple free energy calculations (Fig. 2e and f) show that the growth of interfacial water nanodroplets from the initial water film is thermodynamically favoured, provided that the nanodroplets reach a size comparable to that observed in Fig. 1 (see ESI section 7 for details†). This indicates that the water nanodroplets form through a nucleation process requiring overcoming an initial interfacial energy barrier. This explanation is also consistent with the dependence on temperature: nucleation being an activated process, its probability usually follows an Arrhenius behaviour[52] and is hence proportional to e^{-A/k_BT} where A is the activation energy and k_B the Boltzmann's constant. Consistently with classical nucleation theory, once the water nanodroplets are formed, they are stable and tend only to grow through ripening. This is visible in the hysteresis behaviour observed when the temperature is brought back down to 25 °C (Fig. 1) with fewer, larger droplets being present at the interface.

We also examined the evolution of the van der Waals interactions between water, hexadecane and mica with temperature. While the interface thermodynamics is the likely driving force for the nanodroplets nucleation, van der Waals interactions may play a role here given the high dieletric constant of

mica.[60,61] As expected, the Hamaker constant describing the van der Waals interaction between hexadecane and mica through water, H_{hwm}, and that describing the interaction between water and mica through hexadecane, H_{whm}, both increase with temperature (see ESI section 8 for details†). However, the increase rate is higher for H_{hwm} so that the ratio H_{whm}/H_{hwm} decreases with temperature (Fig. 2g). While the effect is small, this further supports the idea that a temperature increase of the system comparatively reinforces the van der Waals interactions between the hexadecane molecules and the mica surface through the interfacial water.

The macroscopic equilibrium perspective

While AFM measurements provide nanoscale insights into the evolution of the interface, the interpretation of the results rely on macroscopic concepts such as the interfacial energies between the different materials constituting the system. We therefore conducted macroscopic measurements of the static contact angle formed by hexadecane and mica at different relative humidity (Fig. 3). To allow for comparison, all the experiments are conducted with the same volume of hexadecane, over a same, freshly cleaved mica surface and at the same temperature. At RH = 0%, hexadecane spreads rapidly over mica. The spreading kinetics can be well described with an exponential convergence to the maximum coverage, yielding a single timescale of 35 ± 5 s (Fig. 3a). Hexadecane is fully wetting with a contact angle close to 0° as for pure water on mica (Fig. 3b). When the relative humidity increases, the hexadecane retains its ability to spread rapidly, at least initially. In all cases, hexadecane strongly wets the interface with a contact angle <10° (Fig. 3b–d) even at saturated humidity (RH = 100%) where the water layer initially present on the mica surface is ~2 nm thick.[46] At RH = 100%, hexadecane spreading kinetics can also be modelled with a single exponential convergence to the maximum coverage (Fig. 3a), returning a slightly slower timescale of 55 ± 5 s compared to RH = 0%. The similarity is not surprising considering the very similar interfacial energies γ for hexadecane-mica ($\gamma_{h,m}$ = 53.90 mN m^{-1}) and hexadecane-water ($\gamma_{h,w}$ = 51.30 mN m^{-1}, see Table S1†). This suggests that the hexadecane uniformly spreads over the unaltered initial water layer, experiencing a thermodynamic situation almost identical to that in a completely dry atmosphere. This is also consistent with thermodynamics considerations whereby the thick water layer present in saturated conditions[46] renders the nucleation of water nanodroplets less favourable (Fig. 2f and Fig. S3†). The final coverage reached over the timescale of the experiment is lower than for RH = 0% simply due to the higher contact angle. The situation is however different for the intermediate relative humidity (RH = 46%) that does not follow the trend. First, its maximum coverage is the lowest despite an intermediate contact angle value. Second, the kinetics is unusual with an initial rapid expansion comparable to that at RH = 0% (timescale of 25 ± 5 s) followed by a slow receding of the hexadecane spread, occurring over hundreds of seconds. This slow recess, highlighted by the exponential fitting (Fig. 3a) points to new interfacial effects absent in the other

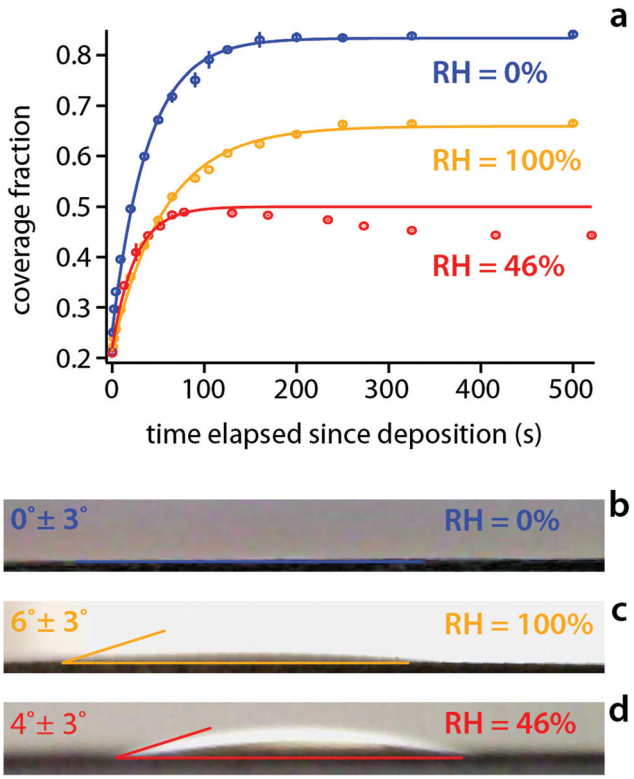

Fig. 3 Wetting dynamics for hexadecane on mica as a function of the relative humidity. (a) The time evolution of the hexadecane surface coverage fraction is tracked for dry (RH = 0%), humidity saturated (RH = 100%) and ambient (RH = 46%) conditions. Each set of kinetic data behaves as a simple exponential convergence to the maximum coverage achieved (solid lines fit) except for RH = 46% where the hexadecane recedes past 100 s. Snapshots of the movies tracking the evolution of the hexadecane drops provide estimate of the contact angle in each case (b–d) (see ESI† for movies of the drop evolution). The error on the RH is ±2%. All the experiments were performed at 25 °C with the mica disc first equilibrated for 30 minutes in the desired conditions before depositing a 5 μl hexadecane drop and immediately recording its evolution.

cases. Given the moderate relative humidity, the water layer initially covering the mica surface is not as thick as for RH = 100% but typically less than 1 nm.[38,39] Occasional water nanodroplets are therefore likely to nucleate over the course of the experiment. However, given the relatively low temperature of the system (25 °C), the nucleation rate is slow and only few droplets nucleate, progressively growing into large droplets by absorbing the surrounding water layer. This effect may render the interface inhomogeneous and hamper even the spreading of the hexadecane into a uniform layer. The small number of interfacial water droplets would also explain the fact that none were observed by AFM in these conditions with their effect only visible at the macroscale when the whole interface is considered.

The possibility of air-born water microdroplets bringing down hydrocarbons from the glove box walls onto the mica surface cannot be excluded, including species containing hydrophilic groups.[51,62] Such molecules could create a bridge

between the adsorbed water layer on mica and hexadecane, enhancing the hexadecane spreading at high humidity. However, the consistency of the nucleation interpretation for macroscopic and molecular-level AFM results suggest the later explanation to be the most likely interpretation.

Molecular impact of water on lubricated friction

It is well-known that water can alter the shear response of a lubricant.[24,63] Water can interfere with the hexadecane molecular packing and self-organisation, and thus reduce the smooth sliding of the AFM probe on the alkane layer.[64,65] Additionally, water molecules create surface singularities where the AFM tip can be subject to pinning.[66] Here, our AFM-based experimental setup allows for precise quantification of the interface's lubrication properties with nanometre lateral resolution. This makes it possible to directly compare areas of uniform hexadecane-mica interface with regions where water nanodroplets are present within a same experiment. Measurements taken directly on nanodroplets exhibit a twofold increase in shear force for any applied load compared to a uniform hexadecane interface in identical conditions (Fig. 4a).

The associated shear phases show the expected viscoelastic behaviour, but with little difference between both situations (Fig. 4b), at least for the shear rate used here. This suggests water to modify primarily the properties of the shearing surfaces, with the viscoelastic behaviour of the confined liquid being dominated by the hexadecane. Indeed, shearing in pure water tends to induce a very different phase behaviour.[12] To confirm this hypothesis, we conducted shear measurements at different temperatures. In pure liquids, the shear force usually decreases with increasing temperature[28,66] and the lubricant tends to become more viscous (shear phase closer to 90°). Here we expect more nanodroplets to nucleate at the interface when the temperature is raised, hence inducing an increase in shear force. Since the AFM measurements are highly localised, for each temperature probed at least 140 force curves were acquired, taken over 7 randomly selected locations and subsequently averaged. The results confirm the increase of shear force with temperature (Fig. 4c and d), reflecting the associated

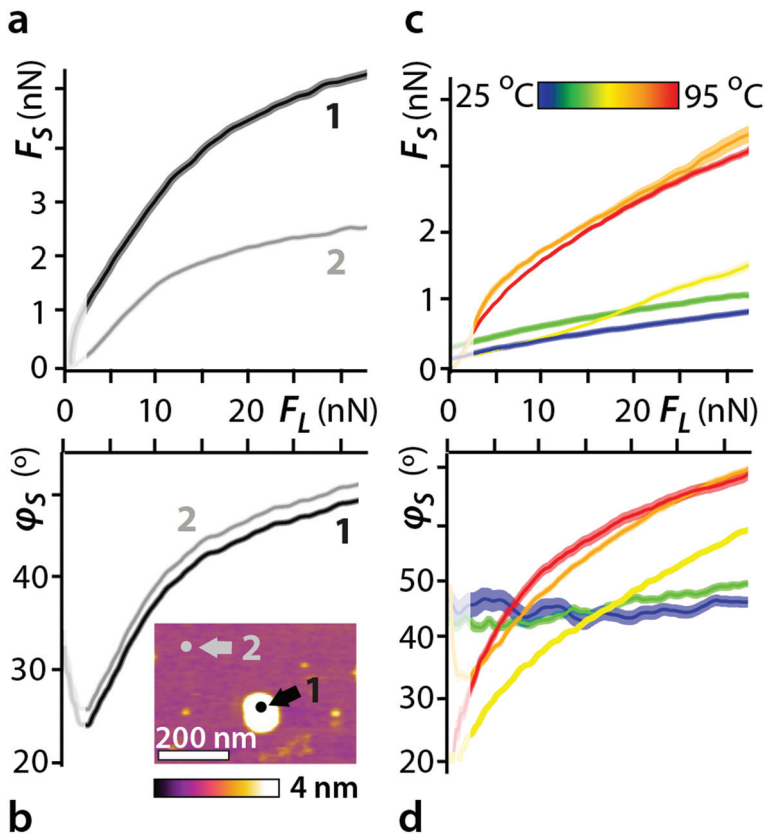

Fig. 4 Impact of water nanodroplets on lubricated friction. Representative shear spectroscopy measurements (a) conducted either on a water nanodroplet (b, inset location 1) or a homogenous hexadecane-mica interface (b, inset location 2). Water nanodroplets induce large changes in the lubricated friction force F_S for a given applied load. The associated shear phase φ_S (b) appears much less sensitive to the location probed. Shear measurements were also conducted at different temperatures (c-d), averaging results over 7 randomly selected locations for each temperature. F_S increases with temperature due to a larger interface coverage with water nanodroplets (c). The shear phase also tends to increase at higher temperatures (d), reflecting the interfacial liquids becoming more fluid (viscous). For low confining forces (<2 nN), the shear amplitude nears to the experimental noise level and the data is deemed unreliable (semi-transparent region). The temperature in (a and b) is 95 °C. The experiments were performed at RH = 42 ± 2%.

higher probability to shear over a water nanodroplet. The effect is non-monotonic with temperature, showing little evolution in shear force and phase between the water and the hexadecane below 55 °C (yellow curve in Fig. 4c and d). This reflects the low probability for the AFM tip to randomly encounter a water nanodroplet.

The significant but localised impact of water nanodroplets on lubrication can be reduced using an amphiphilic molecule to decrease the interfacial energy of the system. Here we use oleic acid, known for its surfactant properties and its ability to form supramolecular structure between water and hexadecane.[67,68] The polar head of oleic acid binds to water, whereas its carbon chain is attracted to hexadecane molecules, thus effectively preventing the latter from displacing the former. We examined the impact of oleic acid on both the nucleation of water droplet at the interface with temperature, and the resulting changes in lubricated friction forces. The results are presented in Fig. 5.

The addition of only 0.01% of oleic acid to the hexadecane (molar concentration) before deposition on the mica surface already decrease the nucleation of water nanodroplets by more than 50% at any temperature explored. Further increasing the molar concentration of the amphiphilic acid to 0.1% results in a fourfold decrease in water nanodroplets when compared with pure hexadecane. If we assume a saturated oleic acid layer standing upright at the interface between the mica surface and the hexadecane, a 0.1% oleic acid molecular concentration would approximately represent a hundred-fold excess to the minimum number of molecules needed to cover the interface (see ESI section 11†). Considering the fact that the molecules are not bound at the interface and the system entropy will inevitably retain some of the oleic acid in the solution, no oleic acid aggregates are likely to be present within the nano-confined hexadecane but instead form a regular layer. Such a layer would also be favoured by the amphiphilic nature of the acid. In addition, the interaction between oleic acid molecules is relatively long ranged,[69] thus not necessarily requiring a full coverage of the initial water layer to be effective. Indeed, 0.01% of acid already has a significant effect on the interface (Fig. 5a and b). The impact of oleic acid on the structural organisation of the water/hexadecane interface has crucial consequences on the shear response of the system. The average lubricated friction markedly decreases as a function of oleic acid concentration (Fig. 5c). The lubrication process also appears to

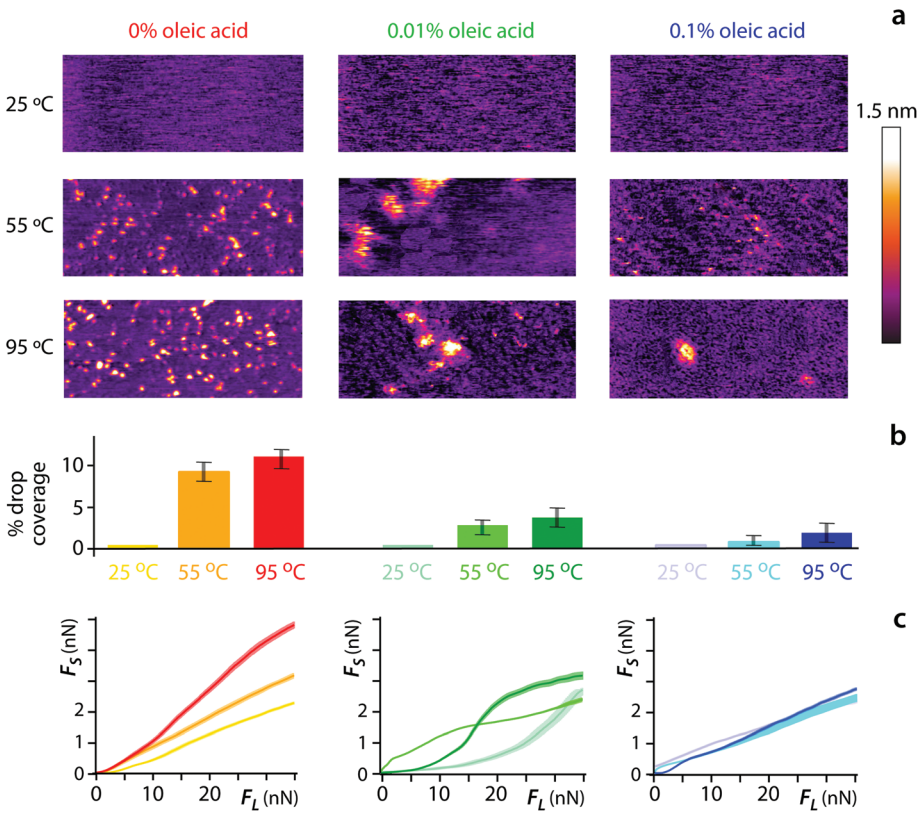

Fig. 5 Reducing the impact of water nanodroplets on lubrication. High-resolution amplitude-modulation AFM imaging of hexadecane-mica interface shows the expected presence of water nano-droplets as the temperature rises (0% oleic acid) (a). However, adding small amounts of oleic acid limits the formation of nanodroplets, with an effect already visible at 0.01 molar percentage. The impact of added oleic acid can be quantified by measuring the percentage of the interface covered with water nanodroplets using a thresholding approach (b). The reduction in interfacial nanodroplets also reduces the shear force and its anomalous behaviour with temperature (c) (see Fig. S9† for the associated phase). All the experiments were performed at RH = 45 ± 2%.

change, with a close to linear dependence of the lubricated friction force on the applied load. This behaviour can be observed in aqueous solutions[12] but is unusual in organic lubricants.[28] This suggests the particular arrangement of the oleic acid at the interface to play a dominating role in reducing friction, not only by removing the water nanodroplets, but also by forming a passivation layer protecting the AFM tip from pinning and playing a lubricating role. Further studies are needed to test the present findings on systems closer to real-life applications such as the metal oxides surfaces,[14,19] routinely used in engines and machinery. At the nanoscale, lubricated friction is likely to result from the combined effects of the molecular arrangement around hydrophilic nano-domains and at topographical defects[66] which may favour the specific pinning of certain molecules. The impact of tribological contacts resulting from the larger roughness inherent to most functioning systems will also need to be taken into account.

Conclusions

In this study, we have investigated the nanoscale details of the impact of ambient humidity on lubricated friction in a well-established model system. The experiments, combining high-resolution AFM imaging and nano-localised shear-force measurements, show that increasing the temperature of the system stimulates the nucleation of water nanodroplets at the hydrophilic interface. A fine balance of interfacial energies between mica, water and hexadecane determine the nucleation threshold, and water nanodroplets become stable for sizes in the range 20–50 nm, depending on the ambient humidity. Interestingly the same thermodynamics calculations used to estimate the nucleation threshold indicate a nucleation threshold with smaller droplets on the less hydrophilic metal oxide typical of engines (see ESI section 7†). This would render the nucleation of water droplets more likely considering the stochastic nature of the nucleation process. Water nanodroplets are highly detrimental to the lubrication properties of the interface by modifying the wetting properties of the shearing surfaces and creating local pinning points. The presence of droplets in engines and machinery that are typically made of metal are likely to exacerbate this effect. The issues can be however mitigated through the adjunction of amphiphilic molecules such as oleic acid to the lubricant, here hexadecane. With its hydrophilic groups, oleic acid binds to the water layer adsorbed on mica, whereas its hydrophobic chain has a strong affinity for the overlying hexadecane fluid. This prevents hexadecane from competing and displacing water molecules from the mica's surface, considerably reducing the average lubricated friction force. Overall, the present results provide a nanoscale description of the different processes at play and help explain the macroscale observations: humidity markedly limits the efficiency of oil-based lubricants on hydrophilic substrates such as the metal surfaces often used in car engines and industrial machinery. The present results may contribute to the rational design of optimal tribological solutions for technological applications.

Conflicts of interest

There are no conflicts of interest to declare.

Acknowledgements

Funding: funding from the Engineering and Physical Sciences Council through the iCASE studentship program (grant EP/P510476/1) (CC) is acknowledged. KV is grateful for support from the Royal Society (RS grant RG140190).

References

1 M. Urbakh, J. Klafter, D. Gourdon and J. Israelachvili, *Nature*, 2004, **430**, 525–528.
2 H. Turlier, D. A. Fedosov, B. Audoly, T. Auth, N. S. Gov, C. Sykes, J.-F. Joanny, G. Gompper and T. Betz, *Nat. Phys.*, 2016, **12**, 513–519.
3 G. D. Jay and K. A. Waller, *Matrix Biol.*, 2014, **39**, 17–24.
4 K. Lormes, J. Schumacher, M. Fahr and J. Müller, *MTZ Worldwide*, 2018, **79**, 50–53.
5 A. Greco, K. Mistry, V. Sista, O. Eryilmaz and A. Erdemir, *Wear*, 2011, **271**, 1754–1760.
6 J. Krim, *Adv.Phys.*, 2012, **61**, 155–323.
7 K. Holmberg, R. Siilasto, T. Laitinen, P. Andersson and A. Jäsberg, *Tribol. Int.*, 2013, **62**, 58–77.
8 D. Berman, A. Erdemir and A. V. Sumant, *Mater. Today*, 2014, **17**, 31–42.
9 Z. Chen, X. He, C. Xiao and S. Kim, *Lubricants*, 2018, **6**, 74.
10 A. E. Filippov, J. Klafter and M. Urbakh, *Phys. Rev. Lett.*, 2004, **92**, 135503.
11 T. E. Fischer, M. P. Anderson, S. Jahanmir and R. Salher, *Wear*, 1988, **124**, 133–148.
12 C. Cafolla and K. Voïtchovsky, *Nanoscale*, 2018, **10**, 11831–11840.
13 K. Hasz, Z. Ye, A. Martini and R. W. Carpick, *Phys. Rev. Mater.*, 2018, **2**, 126001.
14 M. Lapuerta, J. Sánchez-Valdepeñas and E. Sukjit, *Wear*, 2014, **309**, 200–207.
15 B. Basu, R. G. Vitchev, J. Vleugels, J. P. Celis and O. Van Der Biest, *Acta Mater.*, 2000, **48**, 2461–2471.
16 Q. Wei, M. Mukaida, W. Ding and T. Ishida, *RSC Adv.*, 2018, **8**, 12540–12546.
17 S. Soltanahmadi, A. Morina, M. C. P. van Eijk, I. Nedelcu and A. Neville, *Tribol. Int.*, 2017, **107**, 184–198.
18 A. Arcifa, A. Rossi, R. M. Espinosa-Marzal and N. D. Spencer, *ACS Appl. Mater. Interfaces*, 2016, **8**, 2961–2973.
19 J. Zhang and H. Li, *Surf. Coat. Technol.*, 2016, **304**, 530–536.
20 J. K. Lancaster, *Tribol. Int.*, 1990, **23**, 371–389.

21 H. Cen, A. Morina, A. Neville, R. Pasaribu and I. Nedelcu, *Tribol. Int.*, 2012, **56**, 47–57.
22 K. Jacques, T. Joy, A. Shirani and D. Berman, *Tribol. Lett.*, 2019, **67**, 105.
23 A. Jabbarzadeh, J. D. Atkinson and R. I. Tanner, *J. Chem. Phys.*, 1999, **110**, 2612–2620.
24 F. Tian, X. Xiao, M. M. T. Loy, C. Wang and C. Bai, *Langmuir*, 1999, **15**, 244–249.
25 R. Pit, H. Hervet and L. Léger, *Phys. Rev. Lett.*, 2000, **85**, 980–983.
26 A. Jabbarzadeh, *Tribol. Int.*, 2016, **97**, 108–115.
27 C. Kajdas, M. Makowska and M. Gradkowski, *Lubr. Sci.*, 2006, **15**, 329–340.
28 K. Voïtchovsky, *Nanoscale*, 2016, **8**, 17472–17482.
29 N. Maeda, M. M. Kohonen and H. K. Christenson, *J. Phys. Chem. B*, 2001, **105**, 5906–5913.
30 O. Y. Fajardo, F. Bresme, A. A. Kornyshev and M. Urbakh, *ACS Nano*, 2017, **11**, 6825–6831.
31 Y. Zhu, H. Ohtani, M. L. Greenfield, M. Ruths and S. Granick, *Tribol. Lett.*, 2003, **15**, 127–134.
32 X. Gong and L. Li, *Adv. Eng. Mater.*, 2018, **20**, 1700617.
33 P. K. Jana, W. Chen, M. J. Alava and L. Laurson, *Phys. Chem. Chem. Phys.*, 2018, **20**, 18737–18743.
34 S. Ohnishi and A. M. Stewart, *Langmuir*, 2002, **18**, 6140–6146.
35 M. D. Krass, G. Krämer, U. Dellwo and R. Bennewitz, *Tribol. Lett.*, 2018, **66**, 87.
36 S. T. Cui, P. T. Cummings and H. D. Cochran, *J. Chem. Phys.*, 2001, **114**, 6464–6471.
37 S. Balasubramanian, M. L. Klein and J. I. Siepmann, *J. Chem. Phys.*, 1995, **103**, 3184–3195.
38 X. Gong, A. Kozbial and L. Li, *Chem. Sci.*, 2015, **6**, 3478–3482.
39 K. Xu, P. Cao and J. R. Heath, *Science*, 2010, **329**, 1188–1191.
40 E. J. Miller, W. Trewby, A. F. Payam, L. Piantanida, C. Cafolla and K. Voïtchovsky, *JoVE*, 2016, **118**, e54924.
41 H. J. Butt and M. Jaschke, *Nanotechnology*, 1995, **6**, 1–7.
42 C. Cafolla, A. F. Payam and K. Voïtchovsky, *J. Appl. Phys.*, 2018, **124**, 154502.
43 K. Voïtchovsky, J. J. Kuna, S. A. Contera, E. Tosatti and F. Stellacci, *Nat. Nanotechnol.*, 2010, **5**, 401–405.
44 J. Schindelin, I. Arganda-Carreras, E. Frise, *et al.*, *Nat. Methods*, 2012, **9**, 676–682.
45 M. Brugnara., *Contact Angle plugin for ImageJ software*, University of Trento, Trento, 2010.
46 T. Arai, K. Sato, A. Iida and M. Tomitori, *Sci. Rep.*, 2017, **7**, 1–11.
47 T. Fukuma, Y. Ueda, S. Yoshioka and H. Asakawa, *Phys. Rev. Lett.*, 2010, **104**, 016101.
48 M. Ricci, P. Spijker and K. Voïtchovsky, *Nat. Commun.*, 2014, **5**, 4400.
49 S. H. Loh and S. P. Jarvis, *Langmuir*, 2010, **26**, 9176–9178.
50 H. K. Christenson and N. H. Thomson, *Surf. Sci. Rep.*, 2016, **71**, 367–390.
51 Z. Li, A. Kozbial, N. Nioradze, D. Parobek, G. J. Shenoy, M. Salim, S. Amemiya, L. Li and H. Liu, *ACS Nano*, 2016, **10**, 349–359.
52 P. G. Debenedetti, *Metastable liquids: concepts and principles*, Princeton University Press, Princeton, 1996.
53 H. D. Ackler, R. H. French and Y. M. Chiang, *J. Colloid Interface Sci.*, 1996, **179**, 460–469.
54 C. J. Van Oss, M. K. Chaudhury and R. J. Good, *Chem. Rev.*, 1988, **88**, 927–941.
55 I. Lee, *J. Mater. Sci.*, 1995, **30**, 6019–6022.
56 F. L. Leite, C. C. Bueno, A. L. Da Róz, E. C. Ziemath and O. N. Oliveira, *Int. J. Mol. Sci.*, 2012, **13**, 12773–12856.
57 R. Pashley and M. Karaman, *Applied colloid and surface chemistry*, John Wiley and Sons, West Sussex, 2004.
58 J. H. Masliyah and S. Bhattacharjee, *Electrokinetic and colloid transport phenomena*, John Wiley & Sons, Boca Raton, 2006.
59 W. M. Haynes, *CRC handbook of chemistry and physics*, CRC press, Boca Raton, 2014.
60 C. G. Low, Q. Zhang, Y. Hao and R. S. Ruoff, *Small*, 2014, **10**, 4213–4218.
61 C. G. Low and Q. Zhang, *Small*, 2012, **8**, 2178–2183.
62 A. Verdaguer, G. M. Sacha, H. Bluhm and M. Salmeron, *Chem. Rev.*, 2006, **106**, 1478–1510.
63 M. Binggeli and C. M. Mate, *J. Vac. Sci. Technol., B: Microelectron. Nanometer Struct.–Process., Meas., Phenom.*, 1995, **13**, 1312–1315.
64 G. Graziano, *Chem. Phys. Lett.*, 2011, **511**, 262–265.
65 Y. Qiu and V. Molinero, *Crystals*, 2017, **7**, 86.
66 C. Cafolla, W. Foster and K. Voïtchovsky, *Sci. Adv.*, 2020, **6**, eaaz3673.
67 H. Fang, W. Wu, Y. Sang, S. Chen, X. Zhu, L. Zhang, Y. Niua and W. Gan, *RSC Adv.*, 2015, **5**, 23578–23585.
68 D. Wu and V. Hornof, *Chem. Eng. Commun.*, 1999, **172**, 85–106.
69 M. H. Wood, M. T. Casford, R. Steitz, A. Zarbakhsh, R. J. L. Welbourn and S. M. Clarke, *Langmuir*, 2016, **32**, 534–540.